Dalton Transactions

An international journal of inorganic chemistry

Accepted Manuscript

This article can be cited before page numbers have been issued, to do this please use: M. Lippi, J. Caputo, F. Meneghetti, C. Castellano, J. Marti-Rujas and M. Cametti, *Dalton Trans.*, 2020, DOI: 10.1039/D0DT02734K.

This is an Accepted Manuscript, which has been through the Royal Society of Chemistry peer review process and has been accepted for publication.

Accepted Manuscripts are published online shortly after acceptance, before technical editing, formatting and proof reading. Using this free service, authors can make their results available to the community, in citable form, before we publish the edited article. We will replace this Accepted Manuscript with the edited and formatted Advance Article as soon as it is available.

You can find more information about Accepted Manuscripts in the Information for Authors.

Please note that technical editing may introduce minor changes to the text and/or graphics, which may alter content. The journal's standard Terms & Conditions and the Ethical guidelines still apply. In no event shall the Royal Society of Chemistry be held responsible for any errors or omissions in this Accepted Manuscript or any consequences arising from the use of any information it contains.

ROYAL SOCIETY OF CHEMISTRY

rsc.li/dalton

View Article Online
DOI: 10.1039/D0DT02734K

ARTICLE

Tuneable Solvent Adsorption and Exchange by 1D Bispidine-Based Mn(II) Coordination Polymers via Ligand Design

Received 00th January 20xx,
Accepted 00th January 20xx

DOI: 10.1039/x0xx00000x

Martina Lippi[a], Josefina Caputo,[a] Fiorella Meneghetti,[b] Carlo Castellano,[c] Javier Martí-Rujas*[a,d] and Massimo Cametti*[a]

[a]Dipartimento di Chimica, Materiali e Ingegneria Chimica, Politecnico di Milano, Via Luigi Mancinelli, 7, 20131, Milano, Italy. E-mail: massimo.cametti@polimi.it; javier.marti@polimi.it

[b]Dipartimento di Scienze Farmaceutiche, Università degli Studi di Milano, Via L. Mangiagalli 25, 20133 Milano, Italy

[c]Dipartimento di Chimica, Università degli Studi di Milano, Via Golgi 19, 20133 Milano, Italy

[d]Center for Nano Science and Technology@Polimi, Istituto Italiano di Tecnologia, Via Pascoli 70/3, 20133 Milano, Italy

Here we report on novel bispidine-based coordination polymers (CPs) **2·TCM**, **3·TCM**, **3·NB**, **5·TCM** and **5·TCM·NB**, of compostition $[Mn(Cl)_2(\mathbf{L2})_2\cdot(TCM)_2]$, $[Mn(Cl)_2(\mathbf{L3})_2\cdot(TCM)_5]$, $[Mn(Cl)_2(\mathbf{L3})_2\cdot(NB)_8]$, $[Mn(Cl)_2(\mathbf{L5})_2\cdot(TCM)_4]$, $[Mn(Cl)_2(\mathbf{L5})_2\cdot(TCM)_2\cdot(NB)_2]$ respectively (NB = nitrobenzene; TCM = chloroform). They were obtained starting from novel bispidine ligands **L2** (dimethyl 7-isopropyl-3-methyl-9-oxo-2,4-di(pyridin-4-yl)-3,7-diazabicyclo[3.3.1]nonane-1,5-dicarboxylate) , **L3** (dimethyl 7-(cyclohexylmethyl)-3-methyl-9-oxo-2,4-di(pyridin-4-yl)-3,7-diazabicyclo[3.3.1]nonane-1,5-dicarboxylate) and **L5** (dimethyl 7-(4-(dimethylamino)benzyl)-3-methyl-9-oxo-2,4-di(pyridin-4-yl)-3,7-diazabicyclo[3.3.1]nonane-1,5-dicarboxylate), The novel CPs were characterized by single crystal (SC-XRD), powder X-ray diffraction (PXRD) and thermal analyses (TGA). We describe their structural and dynamic properties in terms of solvent exchange and adsorption processes, and we outline the general trends observed on the basis of a total of 16 X-ray structures (4 new) and 21 microcrystalline powder phases (10 new), obtained so far for CPs by coordination of ligands **L1-L5** (Scheme 1), having different substitution at the *N7* position. This large set of CPs comprises monosolvated, bisolvated and desolvated species, and it constitutes a good demonstration of how small differences in the functionalization of the organic ligand can have a strong impact on the resulting structural and dynamic properties of this class of 1D CPs.

1. Introduction

Characterized by regular and modular structures, coordination polymers[1] (CPs) represent a class of hybrid metal-organic materials self-assembled from two components: metal ions and organic ligands. By a judicious choice of these two interacting species in terms of their shape, functionalities and coordination preferences, a large variety of different structures with useful properties can be prepared.[2] Gas adsorption, separation and sensing are most frequent applications of these materials, where CP have indeed achieved significant successes.[3a-f] However catalysis, magnetism, proton conductivity and drug delivery represent areas in which CPs are getting momentum, fuelling additional interest in the field of functional materials.[3g-i] One class of CPs is constituted by one-dimensional (1D) systems characterized by extended linear chains.[4] Despite being considered of generally lower stability[5] when

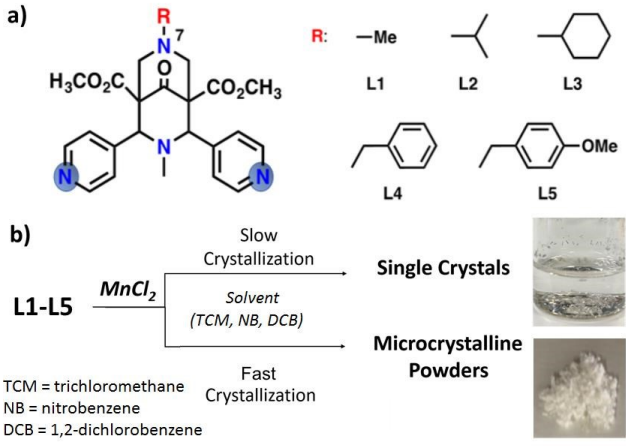

Scheme 1. (a) Molecular formulae of bispidine derivatives **L1-L5**; (b) Synthetic routes for the preparation of the corresponding CPs in microcrystalline and SC forms.

[a] Dipartimento di Chimica, Materiali e Ingegneria Chimica, Politecnico di Milano, Via Luigi Mancinelli, 7, 20131, Milano, Italy. E-mail: massimo.cametti@polimi.it; javier.marti@polimi.it
[b] Dipartimento di Scienze Farmaceutiche, Università degli Studi di Milano, Via L. Mangiagalli 25, 20133 Milano, Italy.
[c] [c]Dipartimento di Chimica, Università degli Studi di Milano, Via Golgi 19, 20133 Milano, Italy.
[d] Center for Nano Science and Technology@Polimi, Istituto Italiano di Tecnologia, Via Pascoli 70/3, 20133 Milano, Italy

Electronic Supplementary Information (ESI) available: [Additional description of the X-ray data (SC- and P-XRD; definition and measurements for δ and ϕ values; NMR data; CCDC 1992169; 2015701-3; 2016611.]. See DOI: 10.1039/x0xx00000x

compared to two-dimensional (2D) or three-dimensional (3D) analogues, 1D CPs are gaining interest due to a relatively easier design, distinct flexibility, enhanced aptitude to transform and specific adsorption capabilities.[6] These attractive features are mainly attributed to the presence of robust 1D arrays, which are held together by weak interactions, building up the overall framework. Highly dynamic CPs are those categorized by Kitagawa as third generation compounds,[7] *i.e.*, systems that reversibly respond to external stimuli of physical and/or chemical nature.[8] Reports by Takamizawa, Vittal, Noro and others,[9] represent splendid examples of guest replacement and selective adsorption processes obtained over the last years with 1D CP systems, which highlight how the crystal flexibility translates into selective responsive behaviour.

Based on this premise, our studies were recently aimed at the development of novel 1D CPs with tuneable adsorption properties. In order to achieve this goal, we envisaged the need of employing relative rigid ligands, whose structure could be easily functionalized. Bispidines, characterized by a rigid diazabicyclononane core, possess all of the abovementioned features. These compounds were firstly synthesized almost a century ago, and they are still attracting attention, in particular as metal binders.[10] Recently, we reported on the first bispidine-based CPs, obtained by orienting the pyridine N donors of the ligand in a divergent fashion, as in **L1** (Scheme 1a), and using Mn(II) ions.[11] SC-XRD analysis revealed the formation of monosolvated 1D CPs characterized by ribbon-like linear arrays made of -[Mn(Cl)$_2$(**L1**)$_2$]- units, and containing chloroform (TCM), nitrobenzene (NB) or dichlorobenzene (DCB) within their lattice. These materials, either as single crystals or microcrystalline powders, proved to be capable to undergo various type of transformations *via* solvent exchange and adsorption processes.

In general, packing efficiencies in solid crystalline materials depend on the shape and flexibility of the building block components.[12] We have already demonstrated for bispidines **L1** and **L4** (Scheme 1), that small structural variations in the ligand structure could influence the dynamic behavior of the corresponding CPs;[11] moreover, we made a prediction by using solid state DFT-calculations based on SC-XRD data of ligands **L1-L5**.[13] Results suggested a tendency of **L4** to create intrinsically more stable, and thus less dynamic CPs, in contrast with those made with **L5**. CPs with **L1-L3** were instead expected to have intermediate properties.

Here, we present our detailed investigation on novel CPs with ligands **L2-L3** and **L5** with Mn(II). SCs of two new monosolvated CPs were obtained (**2·TCM^{SC}** and **5·TCM^{SC}**), together with a new bisolvated CP (**5 ·TCM·NB^{SC}**). These structures were described and put in a wider context, as we here provide a comprehensive analysis on the totality of 16 SC structures of Mn(II) bispidine-based CPs, comprising mono-, bi- and desolvated species. In addition, we studied these CPs in the form of microcrystalline powder phases, in terms of their capability to undergo solvent exchange and adsorption processes, and by thermal treatment. Our final aim was to make a general comparison between all the CPs obtained so far with the series of ligands **L1-L5**, to highlight common features and marked differences in terms of structure and adsorption capability and to finally provide a clear example on how to successfully modulate the properties of a family of 1D CP systems by ligand modification.

2. Results and discussion

2.1 SC-XRD characterization of Mn(II) bispidine based CPs.

Crystallization under different solvent-mixture conditions using a three-layers crystallization method (see Experimental Section) yielded monosolvated and bisolvated structures, always containing linear ribbon-like arrays.[11, 13, 14] In particular, the monosolvated CPs **1·TCM^{SC}**, **1·NB^{SC}**, **4·TCM^{SC}** and **4·NB^{SC}**, were fully characterized. Within the same family of monosolvated species, two additional CPs containing DCB were obtained. Bisolvated CPs, **4·oNT·TCM^{SC}** (oNT=*o*-nitrotoluene) and **4·pClT·TCM^{SC}** (pCT=*p*-chlorotoluene), were also obtained**.** In addition, the structure of a solvent-free CP, **4**, was determined by *ab-initio* powder X-ray diffraction solution from synchrotron

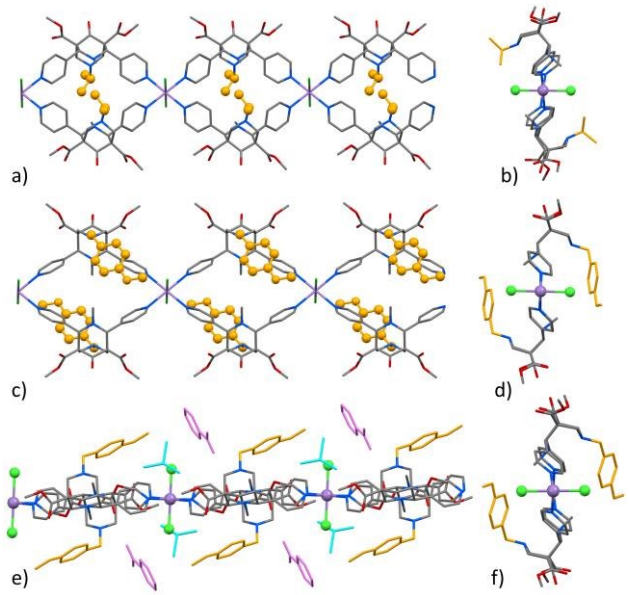

Figure 1. Views of the crystal structures of novel mono- and bi-solvated CPs: ribbon-like 1D array of **2·TCM^{SC}** represented along a) x-axis and b) its propagation direction; ribbon-like 1D arrays of **5·TCM^{SC}** represented along c) x-axis and d) its propagation direction; ribbon-like 1D arrays of **5·TCM·NB** seen along e) x-axis and f) its propagation direction; Colour code: C= orange; H= white; N= blue; Mn=Purple; Cl = green; substituent R (Scheme 1) is shown in orange. In Fig.1e, solvent molecules of TCM and NB are shown in cyan and purple colour, respectively.

data.[14]

In this work, the structures of **2·TCM^{SC}** and **5·TCM^{SC}**, as novel monosolvated CPs, and of **5·NB·TCM^{SC}**, belonging to the bisolvated ensemble, are described, as well as that of **4-oNT^{SC}**, obtained for sake of comparison.

2.1.1 Crystal structure description of 2·TCM^{SC}

Single crystal X-ray crystallography reveals that **2·TCM^{SC}** (ESI) crystallizes in the triclinic system in the *P*1 space group. The

View Article Online
DOI: 10.1039/D0DT02734K

asymmetric unit contains one $MnCl_2$ and two ligands and two included guest TCM molecules; the coordination geometry of Mn(II) is octahedral. The 1D ribbons in **2·TCM^{SC}** are formed through the coordination linkage of repeating 24-membered macrocycles (Figure 1a) which expand into linear arrays (Figure 1b), parallel to each other. The methyl ester groups, present in the rigid core of the bispidine, are oriented *syn-anti* and they play a significant role in the formation of molecular interactions with other 1D ribbons and trapped solvents. There is a weak isopropyl-carbonyl interaction ($d_{H40C\cdots O1}$ = 2.567 Å; 132.66°) among neighboring chains. Regarding the included solvent in **2·TCM^{SC}**, one of the two TCM molecules is in contact with the Mn–bound chloride *via* C–H···Cl interactions (d_{H1-Cl2} = 2.521 Å; 165.36°). The voids space occupied by the two TCM guest molecules, showing no solvent-solvent interactions, is about 16 % of the total unit cell volume (237 Å^3),[15] and characterized by non-interconnected pockets.

Table 1. Name and composition of the CPs obtained as SC mentioned in the text.

CP Name	Composition
1·TCM^{SC}	$[Mn(Cl)_2(\mathbf{L1})_2\cdot(TCM)_2]$
1·NB^{SC}	$[Mn(Cl)_2(\mathbf{L1})_2\cdot(NB)_3]$
1·DCB$^{SC\text{-}I}$	$[Mn(Cl)_2(\mathbf{L1})_2\cdot(DCB)_8]$
1·DCB$^{SC\text{-}II}$	$[Mn(Cl)_2(\mathbf{L1})_2\cdot(DCB)_3]$
1·DCB$^{SC\text{-}III}$	$[Mn(Cl)_2(\mathbf{L1})_2\cdot(DCB)_2]$
2·TCM^{SC}	$[Mn(Cl)_2(\mathbf{L2})_2\cdot(TCM)_2]$
3·TCM^{SC}	$[Mn(Cl)_2(\mathbf{L3})_2\cdot(TCM)_5]$
3·NB^{SC}	$[Mn(Cl)_2(\mathbf{L3})_2\cdot(NB)_8]$
4·NB^{SC}	$[Mn(Cl)_2(\mathbf{L4})_2\cdot(NB)_2]$
4*	$[Mn(Cl)_2(\mathbf{L4})_2]$
4·TCM^{SC}	$[Mn(Cl)_2(\mathbf{L4})_2\cdot(TCM)_4]$
4·*o*NT^{SC}	$[Mn(Cl)_2(\mathbf{L4})_2\cdot(o\text{NT})_2]$
4·TCM·*o*NT^{SC}	$[Mn(Cl)_2(\mathbf{L4})_2\cdot TCM\cdot o\text{NT}]$
4·TCM·*p*Cl^{SC}	$[Mn(Cl)_2(\mathbf{L4})_2\cdot TCM\cdot p\text{CT}]$
5·TCM^{SC}	$[Mn(Cl)_2(\mathbf{L5})_2\cdot(TCM)_4]$
5·TCM·NB^{SC}	$[Mn(Cl)_2(\mathbf{L5})_2\cdot(TCM)_2\cdot(NB)_2]$

*characterized by *ab initio* structure solution from synchrotron powder diffraction data.[14]

2.1.2 Crystal structure description of 5·TCM^{SC} and 5·NB·TCM^{SC}

The two new SC of 1D CPs were obtained by reacting ligand **L5**,[16] which has a *p*-methoxybenzyl group at the *N*7 position, with Mn(II) ions (ESI). The first structure with **L5** (**5·TCM^{SC}**) contains half $MnCl_2$, one ligand (**L5**) and two guest TCM molecules in the asymmetric unit. The coordination geometry of Mn(II) is octahedral as in **2·TCM^{SC}** and the 1D ribbons (Figures 1c and 1d) are also running parallel to each other. At variance with **2·TCM^{SC}**, solvent molecules occupy small 1D channels that expand along the [101] crystallographic direction, which correspond to ca. 28 % of the total unit cell volume (548 Å^3).[15] In the third 1D CP built with **L5** (**5·TCM·NB^{SC}**) (ESI), there is half $MnCl_2$ unit, one ligand **L5**, one TCM and one NB guest molecule in the asymmetric unit. The 1D ribbons observed in this CP (Figures 1e and 1f) are also not interwoven and the void space, occupied by the two included guest molecules, corresponds to the 26 % of the total unit cell volume (483 Å^3). The voids form contorted 1D channels: this arrangement is different with respect to the two previous reported bisolvated structures.[14] More structural details are reported in the ESI.

2.2 General overview on the X-ray structural data[17]

From the structural point of view, all the CPs belonging to this family of materials have some common features. First, they are all 1D CPs, with the Mn(II) centers bound to four different bispidine ligands through their divergent pyridine nitrogen donors, forming a distorted octahedral environment with two chloride atoms in the apical positions. Second, the CPs display linear non-interwoven 1D arrays made of –[$MnCl_2(L)_2$]– repeating units, where each ligand pair generates a 24-membered macrocycle. No solvent is ever found within the macrocyclic central cavity, which is probably too small. Third, the 1D ribbons pack entrapping a variety of solvents between adjacent ribbons (NB, DCB, oNT, pCT and TCM). Considering the crystallization conditions,[11] it can be said that MeOH and THF have no tendency to be trapped within the CP lattice.

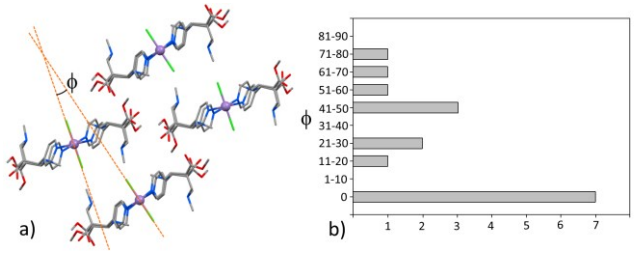

Figure 2. a) Typical packing of the 1D CPs ribbons, shown along the propagation direction; angle ϕ between lines indicates relative ribbon orientation (ϕ=28° in **1-TCM**); b) bar-plot of the inter-ribbon orientation angle ϕ (ESI).

Solvent identity has a major effect on the relative orientation among adjacent 1D ribbons. Figure 2a shows a typical packing, while the bar plot in Fig. 2b indicates the distribution of the orientation angle ϕ (from 0 to 82°), observed among the CP series. The most frequent situation occurring is that with CPs having all the ribbons assembled parallel to each other (7 out of 15 times). Interestingly, all structures with **L1** showed a certain degree of tilting, which varies considerably (from 14° to 82°), while those made with **L2**, **L3** and **L5** have all parallel ribbons. CPs with **L4** displayed a mixed behavior, as they can be found both with no tilting, or with a marked inter-ribbon orientation (from 48 to 65°). These differences in the packing are clearly due to the change of the solvent and ligand. The effect of solvent identity on the spatial organization of the CP ribbons into the overall framework can be clearly highlighted by

the comparison between the structures **4·NB^{SC}** and **4·oNT^{SC}**, where the trapped solvent molecules structurally differ for just an additional methyl group in oNT. In both CPs, the solvents are interacting with the Mn-bound chlorides (CH_{Ar}---Cl = 2.728 Å for **4·NB^{SC}** and CH_{Ar}---Cl = 2.887 Å for **4·oNT^{SC}**), and with each other, forming linear chains. However, while NB molecules can form planar 1D stripes by mutual CH_{Ar}-O_{NO2} HBs ($d_{CHAr\text{-}ONO2}$ = 2.633 and 2.642 Å), that is prevented for oNT. Thus, oNT molecules give rise to a more compact array, extending along a different direction (ESI). Overall, the packing for **4·oNT** leads to ribbons oriented at ca. 44° (compared to ca. 65° for **4·NB**) (ESI). Different ribbon orientation should be correlated with the CPs dynamic behavior. However, no simple way to link the orientation angle ϕ to the CP property can be found.

A different general comparison between the 16 different CPs crystal structures can be drawn also by analysing the observed average close-neighbour inter-ribbon distances δ (Å), reported in Figure 3. Depending on angle α (inset of Figure 3, see ESI), the linear ribbons assembled in two different environments, where each ribbon was surrounded by either six or eight other ribbons in a cubic or hexagonal arrangement, respectively (see ESI).[18] Some of the CPs have a channelled structure into which solvent molecules reside (label **c**, Figure 3), while others are characterized by not-interconnected pockets filled with solvents (label **p**, Figure 3). This plot takes into consideration all the Mn(II)-based CPs obtained so far with the ligands shown in Scheme 1.[17] In our view, δ values are intrinsically related to the stability of the CPs; therefore, we expect higher δ values for the more dynamic CP systems, but deviations from this pattern cannot be *a priori* excluded, as any specific feature of each CP (*i.e.*, solvent content and identity) could have a determining role.

CPs **1·TCM^{SC}** and **2·TCM^{SC}** offer a first direct comparison because they are characterized by: i) same solvent trapped, ii) same type of solvent residency in pockets (see ESI) and iii) a cubic packing. Not surprisingly, **1·TCM^{SC}** and **2-TCM^{SC}** showed very similar δ values, hinting at a negligible effect of the isopropyl groups (*vs* Me). Conversely, **4·TCM^{SC}** has a lower δ value, hinting at a higher stability. However, it also features a different ribbon arrangement and tight 1D channels, extending as alternate layers, instead of pockets (ESI). Interestingly, **4·TCM^{SC}** has closer ribbons, despite having twice the amount of trapped TCM solvent than **1·TCM^{SC}** and **2·TCM^{SC}** and a more sterically demanding substituent (benzyl *vs* methyl or isopropyl). It also undergoes a fast solvent release process at r.t., which generates a completely desolvated phase **4^{Pwd}**,[14] which features the second smallest δ value of the entire series. However, **4·TCM^{SC}** can be directly compared with **3·TCM^{SC}** and **5·TCM^{SC}**. The latter displays a higher δ value, although characterized by the same ribbon packing and similar solvent occupancy of **4-TCM^{SC}**. This can be related to the presence of the OMe group and suggests a looser packing. Of note, **3-TCM^{SC}**, despite the highest solvent content and void space among the monosolvated CPs with TCM, has a δ value lower than that of **5·TCM^{SC}**. In this case, this might be due to the change of the ribbon structure, which adopts a more marked waved character (ESI).

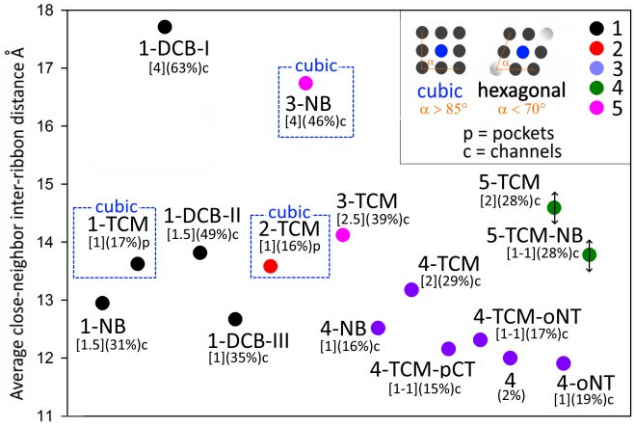

Figure 3. Plot of the average close-neighbor inter ribbon distances, δ, for the 16 SC structures obtained with ligands **L1-L5** and Mn(II) ions. Cubic or hexagonal ribbon arrangement, number of solvent molecules per ligand unit within square brackets [], void space within brackets () and type of solvent occupancy (c = channels; p = pockets) are highlighted. All SC X-ray data were collected at rt except for **5·TCM^{SC}** and **5·TCM·NB^{SC}** measured at 120 K. Details on how to measure δ and α are described in the ESI.

Regarding the NB containing CPs, **1·NB^{SC}** and **4·NB^{SC}** have also a hexagonal packing, with the latter CP ribbons more tightly assembled. A striking difference is observed in **3·NB^{SC}**, which features the second highest δ value, clearly due to the large number of solvent molecules per ligand unit (four).

As far as the bisolvated CPs are concerned, comparison is less reliable due to the presence of different solvents. Nevertheless, they all possess channels; however, **5·TCM·NB^{SC}** displays larger voids (more than 30%) than the other two species, indicating a markedly less efficient ribbon packing, hence a higher δ value.

The effect of the solvent amount within the lattice on the δ value is evident in the three CPs structures with **L1**, entrapping DCB. Upon increase of the solvent content from 1 to 1.5 and to 4 molecules per ligand a monotonous increase of δ values from 12.67 Å to 13.81 Å and to 17.71 Å, respectively, is observed. The latter δ value being the highest within the whole series.

Interestingly, the presence of aromatic solvents induces the formation of channelled structures in all cases. This effect can be accounted for in the cases of **4·NB^{SC}**, where the NB molecules form linear antiparallel side-to-side arrays, and in the CPs where the large amount of solvent clearly opens up the entire framework. In the bisolvated cases, there are no measurable solvent-solvent interactions, although the solvent molecules are arranged into alternate columns (**4·TCM·pCT^{SC}** and **4·TCM·oNT^{SC}**), or with TCM separating π-stacked NB pairs (**5·TCM·NB^{SC}**) (ESI).

In general, CPs with **L4** are found in the lower part of the plot, hinting at a higher intrinsic packing stability, despite having the second largest substituent. Compared to CPs made with **L4**, those formed with **L5** are found in the upper part of the mid-plot region (that with δ within ca. 12-15 Å, and containing 12/16 of the CP species), hinting at a lesser stability.

2.3 Microcrystalline powder samples: solvent exchange and adsorption experiments; thermal stability.

1D bispidine-based CPs were obtained also in the form of microcrystalline powders. In an earlier work, the synthesis and characterization of CPs with ligands **L1** and **L4** were fully described.[11] In particular, PXRD, NMR and Thermogravimetric Analysis (TGA) were used to identify each crystalline phase (in combination with simulated PXRD patterns obtained from SC data); moreover, we studied their thermal stability. Microcrystalline powders of **1·TCM^{Pwd}**, **1·NB^{Pwd}**, **4·TCM^{Pwd}**, **4·NB^{Pwd}**, **4·oNT·TCM^{Pwd}** and **4·pClT·TCM^{Pwd}** were structurally consistent with their corresponding SC phases. PXRD patterns of CPs containing DCB (**1·DCB^{Pwd-I}** and **1·DCB^{Pwd-II}** and **2·DCB^{Pwd}**) did not resemble the simulated ones of any crystal structure and remained structurally unknown, although the presence of 1D ribbons was ascertained. The dynamic behaviour of all the above-mentioned CPs in the form of powders, and of the solvent-free phase **4**, was evaluated by guest exchange and selective adsorption tests.

Here, we present the data relative to CPs with ligands **L2**, **L3** and **L5**.

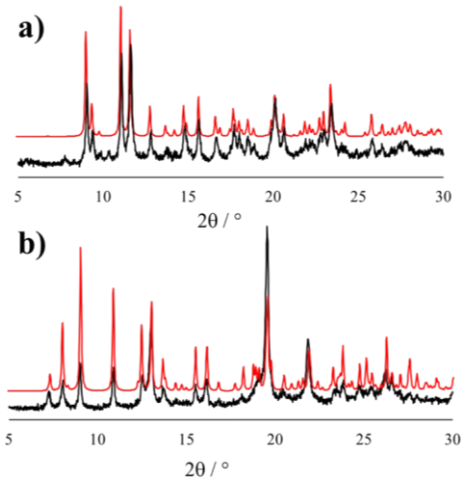

Figure 4. a) PXRD pattern of experimental powder sample **2·TCM^{Pwd}** (black) overlapped with the simulated of **2·TCM^{SC}** (red); **b)** PXRD pattern of experimental powder sample **5·TCM^{Pwd}** (black) overlapped with the simulated of **5·TCM^{SC}** (red).

2.3.1 Dynamic behaviour of 2·TCM and 5·TCM

Fast synthesis with **L2** and **L5** produced four different crystalline phases. Fast crystallization process, using TCM as a solvent, led to crystalline phases whose PXRD patterns agreed with the simulated from SCXRD data of **2·TCM^{SC}** and **5·TCM^{SC}**.
Therefore, these new powder phases were called **2·TCM^{Pwd}** and **5·TCM^{Pwd}** (Figure 4).
By fast crystallization using NB as guest molecule, other two crystalline phases were obtained. Initially, they remained unidentified due to the lack of proper reference SC data (we did not obtain good quality SCs for L**2** or L**5** with NB). However, they are constituted by 1D CPs, as demonstrated by solvent exchange experiments, thus they were named **2·NB^{Pwd-I}** and **5·NB^{Pwd}**. Indeed, the diffractograms obtained after they have been dipped or exposed to TCM for 24 hours resemble the two simulated phases of **2·TCM^{SC}** and **5·TCM^{SC}**, respectively (Figure 5).[19] Notably, the apparent kinetic of these transformations resulted to be relatively fast, indicating that both CPs have a strong tendency to react to external stimuli. We checked also the reversibility of these transformations. The PXRD pattern obtained after dipping **2·TCM^{Pwd}** in NB, showed a new phase which, however, did not match to the pattern of **2·NB^{Pwd-I}**, despite the presence of NB, as confirmed by NMR analysis (Figure S30). This additional unidentified new crystalline phase called **2·NB^{Pwd-II}**, after being dipped in TCM overnight, converts again to **2·TCM^{Pwd}**, indicating the presence of 1D ribbons. On the contrary, the same guest exchange experiment carried out by a solid/gas process, *i.e.* by exposing **2·TCM^{Pwd}** to vapours of NB for two weeks showed the formation of a new crystalline phase, whose PXRD pattern cannot be attributed to any pattern already obtained (not to **2·NB^{Pwd-I}**, nor to **2·NB^{Pwd-II}**) (Figure 6). NMR analysis (Figure S29) on this sample showed the presence of TCM as well as that of NB, and this phase was named **2·NB·TCM^{Pwd}**. This material could represent an intermediate phase, for NB might require more time to completely replace TCM, or a stable product. This latter hypothesis can be sustained by the fact that we have already reported other similar bisolvated bispidine-based CPs.[14]

Similar results came out from the solid/liquid exchange processes of **5·TCM^{Pwd}**, since the resulting PXRD pattern

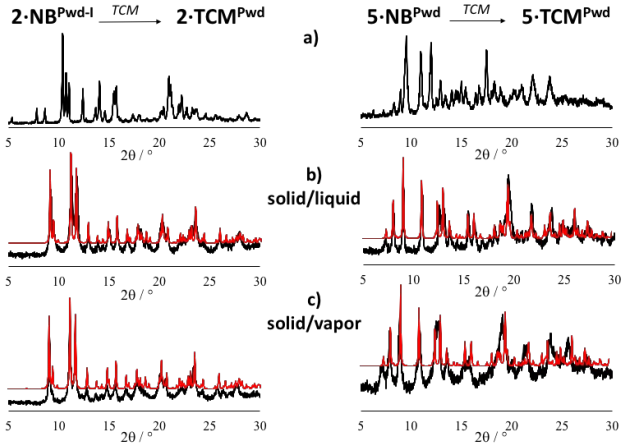

Figure 5. a) PXRD of the starting material, **2·NB^{Pwd}** (left) and **5·NB^{Pwd}** (right); **b-left)** overlapping between the PXRD of the resulting phase obtained by dipping **2·NB^{Pwd}** in TCM for 24 hours (black) and the simulated PXRD of **2·TCM^{SC}**; **b-right)** overlapping between the XRPD of the resulting phase obtained by dipping **5·NB^{Pwd}** in TCM for 24 hours (black) and the simulated XRPD of **5·TCM^{SC}**; **c-left)** overlapping between the PXRD of the resulting phase obtained by exposing **2·NB^{Pwd}** to TCM vapours for 24 hours (black) and the simulated PXRD of **2·TCM^{SC}**; **c-right)** overlapping between the XRPD of the resulting phase obtained by exposing **5·NB^{Pwd}** to TCM vapours for 24 hours (black) and the simulated PXRD of **5·TCM^{SC}**

changed affording a new quite crystalline phase named **5·TCM·NB^{Pwd-I}**, whose NMR spectra showed the uptake of NB, while clearly maintaining the TCM presence (Figure S35). Furthermore, the similarity of **5·TCM·NB^{Pwd-I}** to the simulated data deriving from the X-ray analysis of a single crystal **5·TCM·NB^{SC}**, where both solvents result trapped in the framework, is evident (Figure 6). **5·TCM·NB^{Pwd-I}** was resilient upon dipping in TCM. On the other hand, **5·TCM^{Pwd}** by

solid/vapor exchange process gave rise to another bisolvated phase **5·TCM·NB^{Pwd-II}** after 14 days.[20]
2·NB^{Pwd-I}, **2·NB^{Pwd-II}**, **2·TCM^{Pwd}** and **5·TCM^{Pwd}** were also tested for the solvent exchange with DCB in order to draw a sounder comparison with CPs containing **L1** and **L4**, tested before with

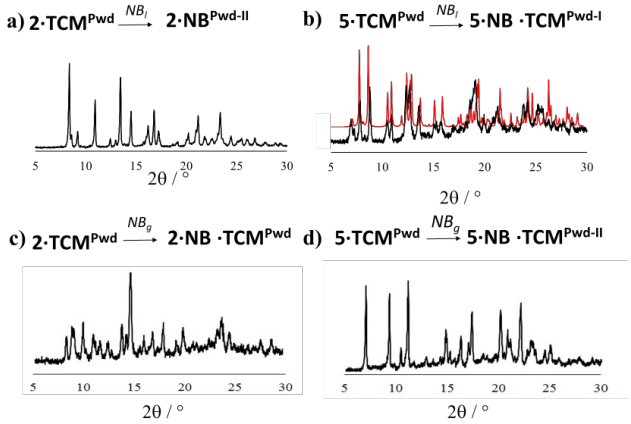

Figure 6. experimental PXRD patterns obtained after: **a**) dipping **2·TCM^{Pwd}** in NB for 24 hours; **b**) dipping **5·TCM^{Pwd}** in NB for 24 hours (overlapped with the simulated pattern of **5·TCM·NB^{SC}** in red**; c)** exposing **2·TCM^{Pwd}** to vapours of NB for 2 weeks; **d)** exposing **5·TCM^{Pwd}** to NB for 2 weeks.

DCB.[11] In the cases of CPs made with **L2**, all the CPs transform, after the exposure to vapours of DCB for 2 weeks. In particular, as shown in Figure 7, the same crystalline phase **2·DCB^{Pwd-II}** was generated by the exposure of both **2·NB^{Pwd-II}** and **2·TCM^{Pwd}** to DCB vapours, while **2·NB^{Pwd-I}** converted to a mixture of **2·DCB^{Pwd-II}** and a novel phase, which was named **2·DCB^{Pwd-I}**. The lack of single crystals X-ray data for CPs including DCB prevents any attribution of these two new microcrystalline phases to a particular CP structure. Nonetheless, these results allow us to reiterate the view of the high dynamic response of CPs made with **L2**. As to CPs of **L5**, all transformations involving an exposure to DCB solvent did not produce phases with good crystallinity (Figures S36 and S37 in ESI).

Unfortunately, for **L3**, the fast crystallization method with Mn(II), applying the same conditions used for the other ligands, yielded amorphous samples. A slight modification of instant synthesis conditions, *i.e.* decreasing the temperature to 0°C, produced the crystalline phases **3·TCM^{Pwd}** and **3·NB^{Pwd}** (see ESI). Notably, exposure of **3·NB^{Pwd}** to vapours of TCM for 2 weeks produced a new crystalline powder sample, containing only TCM (NMR analysis, Figure S31). Also in this case, we did not deepen the study of these materials, due to the absence of a proper structural reference from SC data.

All these results confirmed a high aptitude of the CPs made with **L2** and **L5** to transform, in response to guest exposure. Inspection of Table 2 which illustrates the results of the heterogeneous solid/liquid and solid/vapor guest exchange experiments, allowed us to derive a general pronounced tendency for CPs made with **L1**, **L2** and **L5** to undergo guest replacement. Furthermore, CPs of **L2** and **L5** demonstrated a slightly more dynamic behaviour compared to CPs with **L1**, as their solvent exchange kinetic appeared to be faster. Indeed, exposed to TCM, **2·NB^{Pwd-I}** and **5·NB^{Pwd}** transformed in the corresponding CPs containing TCM after 24 hours of exposure, while for **1·TCM^{Pwd}** two weeks were needed for the exchange to occur. Instead, CPs of **L4** are less inclined to release the original guest and accommodate a new one.

2.3.2 Thermal Stability

The thermal stability of these CPs was also investigated. We considered the response to the thermal treatment, in terms of the crystallinity of the final material, as an indicator of the CP ability to structurally rearrange, or rather collapse, due to solvent loss and/or thermal energy provided.

Thermal responses of the CPs prepared with **L2** and **L5** were

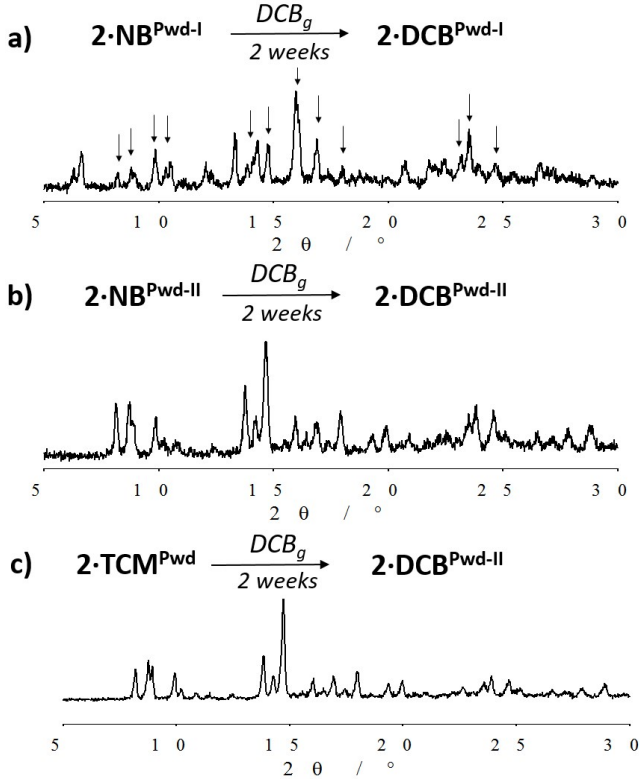

Figure 7. Experimental PXRD pattern obtained after exposing **2·NB^{Pwd-I}** (a), **2·NB^{Pwd-II}** (b) and **2·TCM^{Pwd}** (c) to vapour of DCB for 2 weeks.

compared to those of **1·TCM^{Pwd}**, **1·NB^{Pwd}** and **4·NB^{Pwd}**. While **1·TCM^{Pwd}** maintains crystallinity even at 150°C (Figure S41), **2·TCM^{Pwd}** shows stability up to 120°C, instead at 150°C the framework became amorphous (Figure S42). NMR analysis demonstrated the presence of a small amount of TCM still at 120°C and the absence of the solvent for the amorphous phases formed at 150°C (Figures S52 and S53). TGA of **1·TCM^{Pwd}** and **1·NB^{Pwd}** indicated a weight loss percentage around 180°C, which is in agreement with the theoretical amount of solvent calculated by the SC-XRD data.[11] TGA curve of **2·TCM^{Pwd}** (Figure S49) showed a weight loss of 19.77 % at ca. 160°C, which also in this case can be correlated to the calculated 18.45% from SC data.

TGA was also performed for **2·NB^{Pwd-I}** (no SC reference data available). Solvent release started at ca. 160°C confirming the slightly lower thermal stability of CPs with **L2** compared to those

made with **L1**; these data allowed to estimate the amount of the solvent trapped within its structure to be 1.5 molecules of NB per ligand,[21] a result in line with the situation found with **1·NB** and expected given the relatively small difference in the ligand substitution (Me vs. *i*Pr).

4·NB^{Pwd} resulted quite stable, behaving like **1·TCM^{Pwd}** and **1·NB^{Pwd}**. At a temperature above 150°C, its TGA revealed a weight loss of 17.36%, in full agreement with the theoretical value of 17.56%. On the other hand, **5·NB^{Pwd}** did not undergo major crystallinity loss up to 120°C, temperature at which the NMR analysis showed a little NB inclusion, while **5·TCM^{Pwd}**, after heating at 80°C, instantly transformed in a different desolvated crystalline phase as confirmed by NMR analysis (Figure S54). This new phase, named **5^{Pwd}**, displayed good thermal stability, maintaining its crystallinity up to 120°C (Figure S46). This finding allows a direct comparison between **5·TCM^{Pwd}** and **4·TCM^{Pwd}**: the latter phase loses solvent at r.t. quite rapidly to generate **4^{Pwd}**. If we disregard kinetic factors, one might imply a lower stability for **4·TCM^{Pwd}** compared to **5·TCM^{Pwd}**. This would be in contrast with the assumptions made considering the δ values (Figure 3), unless phase **4** were more stable than **5**, and were this feature be the one driving the transformation (vide infra).

Upon further heating (up to 150°C) **5·TCM^{Pwd}** behaved as **5·NB^{Pwd}**, giving rise to the powder pattern of **L5** (Figure S46) and suggesting that both CPs of **L5** undergo destruction of the polymeric structure at high temperature.[22] Unfortunately, TGA of **5·TCM^{Pwd}** (Figure S50) did not show a weight loss % at 80°C consistent with the expected theoretical value. TGA data for **5·NB^{Pwd}** (Figure S51) allowed instead to estimate ca. three molecules of NB per asymmetric unit.[23] This finding shows a marked difference between CPs with **L4** and those with **L5** (**4·NB^{Pwd}** contains one NB molecule per ligand).

The above described thermal stability and TGA tests are experimental procedures carried out under different conditions; however, collectively, all these data can be used to have an idea of the CP tendency for releasing solvent and of the microcrystalline phase stability related to the solvent loss. Thus, the solvent molecules appear to be more strongly attached to

Table 2. General overview on the guest exchange behaviour of all 1D bispidine-based CPs experimentally obtained as microcrystalline powder samples for ligands **L1**, **L2**, **L4** and **L5**.

Powders samples	***SC references***	***Guest exchange transformation***	
		Solid/liquid (24 hours)	*Solid/vapour (2 weeks)*
1·TCM^{Pwd}	*yes*	• *converts into **1·NB^{Pwd}**.*	• *Converts into **1·NB^{Pwd}***
1·NB^{Pwd}	*yes*	• *converts into **1·TCM^{Pwd}**.* • *converts into **1·DCB$^{Pwd-III}$**.*	• *converts into **1·TCM^{Pwd}**.* • *converts into **1·DCB$^{Pwd-III}$**.*
1·DCB^{Pwd-I}	*no*	• *converts into **1·NB^{Pwd}**.*	• *exchanges NB converting into **1·NB^{Pwd}**.*
1·DCB^{Pwd-II}	*no*	• *converts into **1·NB^{Pwd}**.*	• *converts into **1·NB^{Pwd}**.*
1·DCB$^{Pwd-III}$	*yes*	• *converts into **1·NB^{Pwd}**.*	• *converts into **1·NB^{Pwd}**.*
2·NB^{Pwd-I}	*no*	• *converts into **2·TCM^{Pwd}**.*	• *converts into **2·TCM^{Pwd}**.* • *converts into **2·DCB^{Pwd-I}**.*
2·NB^{Pwd-II}	*no*	• *converts into **2·TCM^{Pwd}**.*	• *converts into **2·NB·TCM^{Pwd}**.* • *converts into **2·DCB^{Pwd-I}**.*
2·TCM^{Pwd}	*yes*	• *converts into **2·NB^{Pwd-II}**.*	• *converts into **2·NB·TCM^{Pwd}**.* • *converts into **2·DCB^{Pwd-I}**.*
4·NB^{Pwd}	*yes*	• *converts into **4·TCM^{Pwd}** .* • *does not transform exposed to DCB.*	• *adsorbs TCM converting into **4·NB·TCM^{Pwd}*** • *does not transform exposed to DCB.*
4·TCM^{Pwd}	*yes*	• *-**	• *-**
4·DCB^{Pwd}	*no*	*(Not performed)*	• *adsorbs TCM converting into **4·DCB·TCM^{Pwd}**;* • *converts into **4^{Pwd}** after exposure to TCM.*
5·TCM^{Pwd}	*yes*	• *converts into **5·NB·TCM^{Pwdl}**.*	• *converts into **5·NB·TCM^{Pwd-II}***
5·NB^{Pwd}	*no*	• *converts into **5·TCM^{Pwd}**.*	• *converts into **5·TCM^{Pwd}**.*

***=** No guest exchange experiments were performed with **4·TCM^{Pwd}** as the material readily converts to **4^{Pwd}** at room temperature.

1·TCM^{Pwd}, **1·NB^{Pwd}** and **4·NB^{Pwd}**, than to the CPs built with **L2** and **L5**; this outcome again supports the greater tendency for these novel CPs to be affected by an external perturbation.

2.3.3 Selective Adsorption Tests

The desolvated phase **5^{Pwd}**, obtained by thermal treatment of **5·TCM^{Pwd}** at 120°C, was considered a suitable candidate for selective adsorption experiments. As mentioned before, we collected strong indications of an enhanced dynamic behavior of CPs prepared with **L5**. Previous experiment established that **4^{Pwd}** had a high resilience to any transformation and it needed a thermal treatment at 150 °C to be activated for adsorption.[11] Notably, we found out that **5 ^{Pwd}** is capable to selectively adsorb NB from various two-solvent mixtures. Indeed, by dipping the starting phase in NB/Toluene, NB/Cl-toluene or NB/1,2-DCB for 24h, a complete transformation into **5·NB^{Pwd}** is observed (Figure 8). These solid/liquid processes did not require any thermal

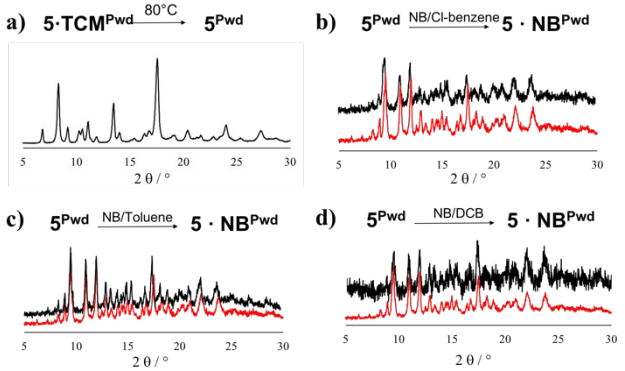

Figure 8. a) Experimental XRPD pattern of **5^{Pwd}** obtained after heating up to 80°C **5·TCM^{Pwd}** in the oven overnight; b) overlapping between the experimental XRPD pattern of **5·NB^{Pwd}** (red) and the experimental XRPD pattern obtained after dipping **5^{Pwd}** in a mixture of NB/chloro-benzene for 24 hours (black); c) overlapping between the experimental XRPD pattern of **5·NB^{Pwd}** (red) and the experimental XRPD pattern obtained after dipping **5^{Pwd}** in a mixture of NB/toluene for 24 hours (black); d) overlapping between the experimental XRPD pattern of **5·NB^{Pwd}** (red) and the experimental XRPD pattern obtained after dipping **5^{Pwd}** in a mixture of NB/DCB for 24 hours (black).

treatment and demonstrated an enhanced aptitude for **5^{Pwd}** to transform by uptaking **NB** compared to **4^{Pwd}**. This finding establishes the enhanced stability of **4^{Pwd}** compared to **5^{Pwd}**, and importantly opens the way to apply this latter phase for separation purposes.

4. Conclusions

Bispidine-based Mn(II) CPs have been extensively explored in terms of their structural features and dynamic properties. In this work, we have completed the studies on the series of ligands **L1-L5**, which differ for the substitution in *N7* position. We have isolated and characterized four new SC X-ray structures of 1D CPs. As far as structural features are concerned, overall, a qualitative analysis over a total of 16 CP structures, comprising monosolvated, bisolvated and desolvated materials was outlined, pointing out differences and similarities, taking advantage of simple metric descriptors (ϕ and θ). Moreover, we evidenced a strong effect of the included solvent on the way CP ribbons orient and pack together.

CPs have been also prepared as microcrystalline powders to test their dynamic properties and thermal stability through PXRD and TGA techniques. A considerable number of different phases have been obtained and proved to be capable to transform *via* solvent exchange or adsorption processes. In particular, CPs made with **L2** and **L5** showed a similar behaviour compared to **L1**, despite the significantly different *N7* substitution (Me and iPr in **L1** and **L2** vs. *p*MeO-benzyl in **L5**). In this regard, the guest response of CPs made with **L4** seems to be outlying. This is especially evident by comparing the selective adsorption capabilities of desolvated microcrystalline **4^{Pwd}** with **5^{Pwd}**. The latter material is indeed dynamic and capable to selectively adsorb NB from NB/Y mixtures (Y = toluene, Cl-toluene or DCB) under solid/liquid heterogeneous conditions.

In general, this work contributes to prove how relatively small ligand structural changes could be employed to finely tune the dynamic behaviour of a family of 1D CP materials.

Given the large number of synthetically accessible structural modifications that can be envisaged for the bispidine ligand, we believe that bispidine-based CPs could become a very promising class of materials with applications in selective adsorption, sensing and even catalysis, and novel avenues in this direction are being currently investigated.

Experimental

CPs in the form of good quality single crystals were obtained by using a three-layer crystallization method followed by a slow evaporation technique. Typically, a chloroform solution of the ligand (0.035 mmol in 2mL) was introduced at the bottom of a 12 mL vial. Then, the intermediate solvent (2-3 mL) was placed gently on the top of the chloroform solution. After that, a methanolic solution of $MnCl_2·4H_2O$ (0.035 mmol in 1mL) was carefully added as a top layer and the vial was closed. Solvents used as intermediate layer: nitrobenzene, tetrahydrofuran, 1,2-dichlorobenzene, p-chlorotoluene or o-nitrotoluene. In approximately 10-15 days, in most cases, small SCs formed. If not, the samples were left to evaporate slowly for an additional period of c.a. 1-2 weeks. SC X-ray analysis was performed using a Bruker Apex II CCD diffractometer, using graphite-monochromatized Mo-Kα radiation (α = 0.71073 Å). Intensity data were corrected for Lorentz-polarization effects and for absorption (SADABS[24]). The structures were solved by direct methods (SIR-97 [25]) and completed by iterative cycles of full-matrix least squares refinement on Fo^2 and ΔF synthesis using the SHELXL-18 [26] program (WinGX suite [27]). The hydrogen atoms bonded to carbon were included at geometrically calculated positions and refined using a riding model. Uiso(H) were defined as 1·2Ueq of the parent carbon atoms for phenyl and methylene residues and 1·5Ueq of the parent carbon atoms for the methyl group. These data can be obtained free of charge via www.ccdc.cam.ac.uk/conts/retrieving.html (or from the Cambridge Crystallographic Data Centre, 12, Union Road, Cambridge CB21EZ, UK; fax: ++44 1223 336 033; or deposit@ccdc.cam.ac.uk). CCDC-2015703 (**2·TCM^{SC}**), CCDC-1992169 (**5·TCM^{SC}**), CCDC-2015702 (**5·TCM·NB^{SC}**), CCDC-2015701 (**4·oNT^{SC}**) contain the supplementary crystallographic data for this paper.

Microcrystalline powder samples of each CPs were instead synthesized by using a fast crystallization method. The addition of a methanolic solution of 0.5 equivalent of $MnCl_2•H_2O$ to a solution of the ligand (0.01 mM) dissolved

in 2.5 mL of NB, TCM, DCB or oNT, or a mixture of NB/TCM, oNT/TCM, pClTol/TCM after about 10 to 30 minutes of stirring at room temperature yielded white crystalline powders as precipitate. They were filtered under vacuum. In some cases, the addition of cold diethyl ether was needed to induce complete precipitation. Yields were in the 62-97 % range, as detailed here: **1·TCM^{Pwd}** = 89 %; **1·NB^{Pwd}** = 97 %; **2·TCM^{Pwd}** = 68 %; **2·NB^{Pwd-I}** = 62 %; **4·NB^{Pwd}** = 92%; **4·TCM^{Pwd}** = 73 %; **4^{Pwd}** = 71 %; **4·TCM·*o*NT^{Pwd}** = 68 %; **4·TCM·*p*ClT^{Pwd}** = 63%; **5·TCM^{Pwd}** = 91%; **5·NB^{Pwd}** = 88 %.

Analysis by means of XRPD was carried out to identify the crystallinity and in some cases the structure, by comparison to the simulated data deriving from the corresponding single crystal X-ray structure. PXRD experiments were carried out at room temperature with a Bruker D2-Phaser diffractometer equipped with Cu radiation (λ = 1.54184 Å) using Bragg-Brentano geometry. ^{1}H NMR (Bruker Avance 400 MHz) was then used to determine the identity (and the amount, in some cases) of the included solvent: the CP was suspended overnight into acetone-*d6* and then filtered by using Acrodisc Syringe Filters with GHP membrane. No dissolution of the CPs, which must be avoided due of the paramagnetic feature of Mn(II) ions, was observed under these conditions.[11] Thermal stability tests were also performed to investigate about the stability of these materials. Each sample was heated up in the oven for 12 hours in a stepwise manner. Firstly, after heating at 80°C for 12 hours the sample was left to cool down to room temperature and then analyzed by PXRD. This procedure was repeated at temperature of 100°C, 120°C, and 150°C. Thermogravimetric analysis (TGA) was obtained by using the SDT Q600 V20.9 Build 20 instrument operating in the 30-400°C range. TGA curves of sample between 35°C and 300°C are reported in the ESI.

Acknowledgements

All authors thank the Alba-CELLS Synchrotron, Barcelona for granting with beamtime (BL13-XALOC beamline) the Proposal Numbers 2018092985. J. M.-R. thanks Politecnico di Milano for funding "Fondo Chiamata Diretta Internazionalizzazione. Prg. Id. 61566"; M. C. thanks MIUR for Fondi di finanziamento per le attività base di ricerca (FFABR).

Notes and references

1. (a) B. F. Hoskins and R. Robson, *J. Am. Chem. Soc.*, 1989, **111** , 5962-5964; (b) M. Eddaoudi, D. B. Moler, H. Li, B. Chen, T. M. Reineke, M. O'Keeffe and O. M. Yaghi, *Acc. Chem. Res.*, 2001, **34**, 319; (c) S. Kitagawa, R. Kitaura and S. Noro, *Angew. Chem. Int. Ed.*, 2004, **43**, 2334. O. M. Yaghi, M. O'Keeffe, N.W. Ockwig, H. K. Chae, M. Eddaoudi and J. Kim, *Nature*, 2003, **423**, 705-714.
2. (a) J. Jian, Y. Zhao and O. M. Yaghi, *J. Am. Chem. Soc.*, 2016, 138, 3255-3265; (b) E.D. Bloch, W.L. Queen, R. Krishna, J.M. Zadrozny, C. M. Brown and J.R. Long, *Science*, 2012, **335**, 6076, 1606-1610.
3. (a) T.K. Maji and S. Kitagawa, *Pure and Applied Chemistry*, 2009, **79**, 12, 2155-2177; (b) T. Fukushima, S. Horike, Y. Inubushi, K. Nakagawa, Y. Kubota, M. Takata and S. Kitagawa, *Angew. Chem., Int. Ed.*, 2015, **48**, 28, 4820-4824; (c) S. W. Jaros, J. Sokolnicki, A. Wołoszyn, M. Haukka, A. M. Kirillov and P. Smoleński, *J. Mater. Chem. C*, 2018, **6**, 1670-1678; (d) W. Huang, J. Jiang, D. Wu, J. Xu, B. Xue and A. M. Kirillov, *Inorg. Chem.,* 2015, **54**, 10524–10526; (e) Z. Hasan and S. H. Jhung, *J. Hazard. Mat.* 2015, **283**, 329–333; (f) P. Kumar, A. Deep, K.-H. Kim and R. J.C. Brown, *Prog. Polymer Sci.,* 2015, **45**, 102-118; (g) C. Janiak, *Dalton Trans*., 2003, 2781-2804; (h) M. L. Foo, R. Matsuda and S. Kitagawa, *Chem. Mater*, 2014, 26, 1, 310-322; (i) H. Furukawa, K. E. Cordova, M. O'Keeffe and O. M. Yaghi, *Science*, 2013, **341**, 974-986.
4. (a) W. L. Leong and J. J. Vittal, *Chem. Rev.*, 2011, **111**, 2, 688-764.
5. There are notable exceptions: (a) J. Martí-Rujas, S. Bonafede, D. Tushi and M. Cametti, *Chem. Commun*., 2015, **51**, 12357; (b) C. D. Wu, W. Lin, *Angew. Chem. Int. Ed.* 2005, **44**, 1958-1961; (c) G. Kumar Kole, A. J. Cairns, M. Eddaoudi, J. J. Vittal, *New J. Chem.,* 2010, **34**, 2392–2395.
6. (a) M. Liu, H. S. Quah, S. Wen, J. Wang, P. S. Kumar, G. Eda, J. J. Vittal and W. Ji, *J. Mat. Chem C.*, 2017, **5**, 2936; (b)M. Cametti, J. Martí-Rujas, Dalton Trans. 2016, 45, 18832-18837; (c) M. Cametti, I. Bargigia and J. Martí-Rujas, *Dalton Trans.* 2016, 45, 1674; (d) I. J. Vitorica-Yrezabal, G. Mínguez Espallargas, J. Soleimannejad, A. J. Florence, A. J. Fletcher and L. Brammer, *Chem. Sci*.,2013, **4**, 696-708.
7. S. Kitagawa, R. Kitaura and S.-I. Noro, *Bull. Chem. Soc. Jpn*., 1998, **71**, 1739.
8. S. Kitagawa and K. Uemura., *Chem. Soc. Rev.*, 2005, **34**, 109-119; (b) K. Seki, *Phys. Chem*, 2002, **4**, 1968-1971; (c) K. U. Ryotaro and Susumu Kitagawa, *Journal of Solid State Chemistry*, 2015, **178**, 2120-2429; (d) S. Horike, S. Shimomura and S. Kitagawa, *Nat. Chem.*, 2009, **1**, 695.
9. (a) F. Yu, D.-D. Li, L. Cheng, Z. Yin, M. H. Zeng and M. Kurmoo, *Inorg. Chem.*, 2015, **54**, 1655; (b) S. Takamizawa, E. Nakata and H. Yokoyama, *Inorg. Chem. Commun.*, 2003, **6**, 763; (c) S. Takamizawa, E. Nakata and T. Saito, *Inorg. Chem. Commun.*, 2003, **6**, 1415; (d) Y. Takasaki and S. Takamizawa, *Chem Commun.*, 2015, 51, 5024-5027; (e) J. K. Kole and J. J. Vittal, *Chem. Soc. Rev.*, 2013, **42**, 1755-1775; (e) K. Takahashi, N. Hoshino, T. Takeda, S. Noro, T. Nakamura, S. Takeda and T. Akutagawa, *Inorg. Chem.*, 2015, **54**, 9423−9431; (f) S. Noro, T. Akutagawa and T. Nakamura, *Chem. Commun*., 2010, **46**, 3134–3136.
10. (a) P. Comba, M. Kerscher, K. Rücka and M. Starke, *Dalton Trans.,* 2018, **47**, 9202; (b) A. Rossetti, S. Landoni, F. Meneghetti, C. Castellano, M. Mori, G. Colombo Dugoni and A. Sacchetti, *New J. Chem.*, 2018, **42**, 12072. (c) P. Comba, M. Maurer, and P. Vadivelu, *J. Phys. Chem. A*, 2008, 112, 50, 13028–13036; (d) P. Comba, Y.-M. Lee, W. Nam and A. Waleska, *Chem. Commun.*, 2014, **50**, 412-414; (e) F. Bruchertseifer, P. Comba, B. Martin, A. Morgenstern, Johannes Notni, M. Starke and H. Wadepohl, *ChemMedChem.* 2020, **15**, 1–11; (f) G. Singh, K. Zarschler, S. Hunoldt,I. Ivette, S. Martínez, C., L. Ruehl, M. Matterna, R. Bergmann, D. Máthé, N. Hegedüs, M. Bachmann P. Comba, H. Stepha, *Chem. – Eur. J.*, 2020, **26**, 1989-2001.
11. A. Rossetti, M. Lippi, J. Martí-Rujas, A. Sacchetti and M. Cametti, *Chem. – Eur. J.*, 2018, **24**, 19368–19372.
12. X. Guo, S. Gen, M. Zhuo, Y. Che, M. J. Zaworotko, P. Cheng and Z. Zhang, *Coord. Chem. Review*, 2019, **391**, 44-68.
13. M. Lippi, J. Caputo, A. Famulari, A. Sacchetti, C. Castellano, F. Meneghetti, J. Marti-Rujas and M. Cametti., *Dalton Trans.*, 2020, **49**, 5965-5973.
14. M. Lippi, M. Cametti and J. Martí-Rujas, *Dalton Trans.,* 2019, **48**, 16756-16763.
15. Voids were calculated using a spherical probe with a radius of 1.2 Å. L. J. Barbour, *Chem. Commun.*, 2006, 1163.
16. Detailed structural information of **5·TCM^{SC}** and **5·TCM·NB^{SC}** can be found in the ESI.
17. Two of the three CPs made with **L1** and DCB (**1·DCB^{SC-I}**, **1·DCB^{SC-II}** and those made with **L3** (**3·TCM^{SC}** and **3·NB^{SC}**) have received only a partial SC-XRD characterization due to low quality dataset, which however well suffices for extracting the needed information for this comparison (ESI).
18. Average inter-ribbon distances δ are calculated as an average of six or eight distances calculated between metal centres on the same plane, or extrapolating the relevant distances by a manual calculation with a reference distance whenever metal centres of adjacent ribbons were displaced and not on the same plane orthogonal to the ribbon direction. The difference in the ribbon arrangement is related to the α angle (inset Figure 3) as can be seen in Figs S7-S23 in ESI. A cubic arrangement was considered for angles higher than 85°, while a hexagonal packing was considered when the angle was lower than 70°.

View Article Online
DOI: 10.1039/D0DT02734K

19. The presence of TCM in the resulting microcrystalline powders was confirmed also by the NMR spectroscopy, see Figures S28 and S32).
20. This new quite crystalline phase is structurally unidentified, however it seems again to contain both solvents, as after two weeks of exposure, TCM and NB are found in approx. 1:1.5 ratio (Figure S34).
21. The first weight loss recorded by TGA corresponds to a percentage of 26.83 %, and 1.5 molecules of NB per asymmetric unit (Figure S48).
22. This transformation which generates the ligand is observed only with **L5**.
23. TGA data indicate an initial weight loss, which was attributed to the evaporation of water and a second one corresponding to 28.51% in weight which is assumed to be related to NB released. Although no comparison to SC-XRD data is available, an estimate of the solvent percentage was however done (3 NB molecules for asymmetric unit).
24. G. M. Sheldrick, SADABS Area-Detector Absorption Correction Program, Bruker AXS Inc., Madison, WI, USA, 2000.
25. Altomare; M. C. Burla, M. Camalli, G. L. Cascarano, C. Giacovazzo, A. Guagliardi, A. G. G. Moliterni, G. Polidori and R. Spagna, *J. Appl. Cryst*., 1999, **32**, 115.
26. Sheldrick, G. M. *Acta Cryst. C*, 2015, **71**, 3-8.
27. L. J. Farrugia, *J. Appl. Cryst*., 2012, **45**, 849.